INTERNATIONAL JOURNAL FOR NUMERICAL METHODS IN FLUIDS, VOL. 20, 641–648 (1995)

NUMERICAL COMPUTATION OF AN IMPINGING JET WITH UNIFORM WALL SUCTION

YUE-TZU YANG

Department of Mechanical Engineering, National Cheng Kung University, Tainan, Taiwan

SUMMARY

The paper presents numerical predictions of a turbulent axisymmetric jet impinging onto a porous plate, based on a finite volume method of solving the Navier–Stokes equations for an incompressible air jet with the K–ε turbulence model. The velocity and pressure terms of the momentum equations are solved by the SIMPLE (semi-implicit method for pressure-linked equation) method. In this study, non-uniform staggered grids are used. The parameters of interest include the nozzle-to-wall distance and the suction velocity. The results of the present calculations are compared with available data reported in the literature. It is found that suction effects reduce the boundary layer thickness and increase the velocity gradient near the wall.

KEY WORDS impinging jet; uniform suction; turbulence model

1. INTRODUCTION

Turbulent impinging jets are frequently encountered in industry and used for the cooling of high-energy electronic components, heat treatment of non-porous metal sheets, cutting, coating and drying of paper and surface cleaning. As a consequence, there is a considerable body of experimental and analytical data available[1–10] which describes the development of the flow within the jet and along the surface onto which it impinges. When the surface is porous, the development of the radial wall jet is affected. In most practical cases, leakage of fluid through the surface will depend on the local static pressure drop across the surface and will therefore vary along the radial direction of the flow.

Limited data do exist for the case where partial suction is applied to the surface and therefore, as a preliminary to looking at a more realistic problem, numerical studies of the effect of a partial uniform suction on the flow of a turbulent impinging jet are presented and compared with the only known experimental data of Obot *et al.*[10]

2. MATHEMATICAL FORMULATION

2.1. Governing equations

The time-averaged Navier–Stokes equations incorporating the Boussinesq turbulent viscosity concept are used in conjunction with the turbulent viscosity defined by the high-Reynolds-number

CCC 0271–2091/95/070648–08

Received March 1994
Revised October 1994

version of the K–ε model of turbulence.[11] The governing equations for axisymmetric flow can therefore be written in the general form

$$\frac{\partial}{\partial x}(r\rho U\phi) + \frac{\partial}{\partial r}(r\rho V\phi) = \frac{\partial}{\partial x}\left(r\Gamma_\phi \frac{\partial \phi}{\partial x}\right) + \frac{\partial}{\partial r}\left(r\Gamma_\phi \frac{\partial \phi}{\partial r}\right) + rS_\phi, \tag{1}$$

where ϕ may represent any of the variables (U, V, K, ε) and S_ϕ is the corresponding source term. All the governing equations and constants used in this study are summarized in Table I. The two turbulence constants C_μ and C_2 have been taken to be those recommended by Launder and Spalding[11] and obtained by fitting experimental data for axisymmetric jets to the model. These modified constants are

$$C_\mu = 0{\cdot}09 - 0{\cdot}04f, \qquad C_2 = 1{\cdot}92 - 0{\cdot}0667f,$$

$$f = \left|\frac{Y}{2\Delta U}\left(\frac{\partial U_{\mathrm{cl}}}{\partial x} - \left|\frac{\partial U_{\mathrm{cl}}}{\partial x}\right|\right)\right|^{0{\cdot}2}, \tag{2}$$

where U_{cl} is the velocity in the direction of the symmetry axis of the flow, Y is the radial width of the mixing region and ΔU is the axial direction velocity difference across the width of this region.

2.2. *Boundary conditions*

Because of the elliptic nature of the governing partial differential equations, boundary conditions are required along all domain boundaries for all dependent variables. The following boundary conditions are specified as shown in Figure 1.

Boundary I: nozzle exit. A uniform nozzle exit velocity profile is assumed with

$$U = U_{\mathrm{n}}, \qquad K = iU_{\mathrm{n}}^2, \qquad \varepsilon = K_{\mathrm{n}}^{3/2}/\lambda r_{\mathrm{n}}, \tag{3}$$

where i is the turbulence intensity (i = 0·004), λ is the length scale constant and r_{n} is the nozzle radius.

Table I. Summary of equations solved

Equation	ϕ	Γ_{s}	S_ϕ
Continuity	1	0	0
x-Momentum	U	μ_{eff}	$-\frac{\partial p}{\partial x} + \frac{\partial}{\partial x}\left(\mu_{\mathrm{eff}}\frac{\partial U}{\partial x}\right) + \frac{1}{r}\frac{\partial}{\partial r}\left(r\mu_{\mathrm{eff}}\frac{\partial V}{\partial x}\right)$
r-Momentum	V	μ_{eff}	$-\frac{\partial p}{\partial r} + \frac{\partial}{\partial r}\left(\mu_{\mathrm{eff}}\frac{\partial U}{\partial r}\right) + \frac{1}{r}\frac{\partial}{\partial r}\left(r\mu_{\mathrm{eff}}\frac{\partial V}{\partial r}\right) - \frac{2\mu_{\mathrm{eff}}V}{r^2}$
Turbulence energy	K	$\mu + \frac{\mu_{\mathrm{t}}}{\sigma_k}$	$\rho G - \rho\varepsilon$
Energy dissipation	ε	$\mu + \frac{\mu_{\mathrm{t}}}{\sigma_\varepsilon}$	$C_1\frac{\rho\varepsilon}{K}G - C_2\frac{\rho\varepsilon^2}{K}$

Here $\mu_t = C_\mu\rho K^2/\varepsilon$, $\mu_{\mathrm{eff}} = \mu + \mu_{\mathrm{t}}$, $G = \nu_{\mathrm{t}}[(\partial U/\partial r + \partial V/\partial x)^2 + 2(\partial U/\partial x)^2 + 2(\partial V/\partial r)^2 + 2(V/r)^2]$, $C_1 = 1{\cdot}44, \sigma_k = 1{\cdot}0, \sigma_\varepsilon = 1{\cdot}3$.

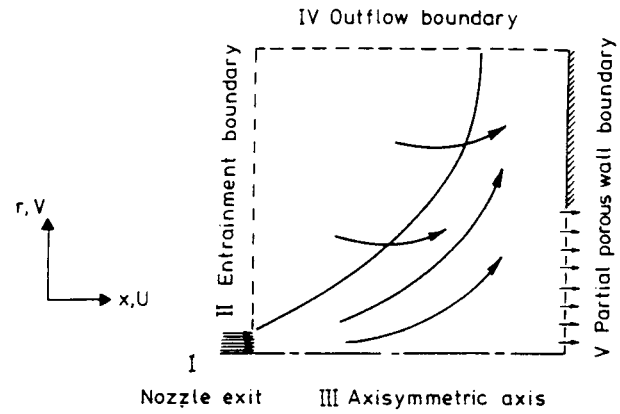

Figure 1

Boundary II: entrainment boundary (constant pressure boundary). Along this boundary the pressure P is taken as the environmental pressure. The velocity normal to the boundary is then calculated by means of the continuity equation.

Boundary III: axisymmetric axis. Along this axis of symmetry the radial gradients of all properties are zero and the radial velocity *V642* is zero, i.e.

$$\frac{\partial U}{\partial r} = 0, \qquad \frac{\partial K}{\partial r} = 0, \qquad \frac{\partial \varepsilon}{\partial r} = 0, \qquad V = 0. \tag{4}$$

Boundary IV: outflow boundary. At this boundary a constant static pressure condition is assumed.

Boundary V: partial porous wall boundary. The wall function method as described by Launder and Spalding[11] for a non-permeable boundary is modified to allow for the effect of suction. For flow over a permeable wall the total shear stress can be represented by[12]

$$\tau = \tau_W + \rho U V_W, \tag{5}$$

Assuming that

$$\frac{\partial U}{\partial y} = \frac{(\tau/\rho)^{1/2}}{\kappa y} \tag{6}$$

and that the integral of (5) and (6) is compatible with

$$\frac{2U\tau}{V_W}\left[\left(1 + \frac{UV_W}{U_\tau^2}\right)^{1/2} - 1\right] = \frac{1}{\kappa}\ln\left(\frac{U_\tau y}{\nu}\right) + C. \tag{7}$$

3. NUMERICAL PROCEDURE

The equations are elliptic and the solution can be obtained numerically by a finite volume scheme as shown in Reference 13. The set of difference equations is solved iteratively using a line-by-line solution method in conjunction with a tridiagonal matrix form. Based on a grid independence study, a 40×42 mesh is used as shown in Figure 2. The solution is considered to be converged when the normalized residual of the algebraic equation is less than a prescribed value of 0·0001. All computations were done on a VAX 9420 computer. The programme converged in about 6000 CPU seconds.

4. RESULTS AND DISCUSSION

The experiments of Obot *et al.*[10] consisted of a uniform jet issuing from a 20 mm diameter (D_n) contoured inlet nozzle impinging concentrically on a 0·97 m diameter plate which was flush with a 348 mm diameter and 9·5 mm thick porous plate. The permeable test plate was mounted in a suction box with its top surface flush with the edges of the suction box. The jet Reynolds number was fixed at 8×10^4, i.e. corresponding to a nozzle exit average velocity of 60 m s^{-1}. The ratio H/D_n had the values 3, 8 and 12 and the suction velocity varied from 0·0 to 0·25 m s^{-1}. The dimensionless velocity profiles U/U_m for $H = 3D_n$ and $8D_n$ are compared for various suction velocities and radial positions in Figures 3 and 4, which present the height y above the impingement surface in terms of $\delta_{1/2}$, where $U(\delta_{1/2}) = \frac{1}{2}U_m$ and U_m is the maximum velocity. For $r/H \geq 1{\cdot}33$ the dimensionless velocity profiles are independent of both suction velocity and radial location as shown in Figure 3, exhibiting almost the same trend as the experimental data. For $r/H \leq 0{\cdot}75$ (Figure 4) the dimensionless profiles show a dependence on location and suction velocity with $V_W = 0{\cdot}0$ m s^{-1}. It can be seen that the calculation is in good agreement with the experimental data except very close to the surface. In this region both the experimental hot wire measurements and the numerical methods are prone to error. The calculated maximum radial velocity (U_m) and wall halfwidth ($\delta_{1/2}$) were in excellent agreement with the experimental data in the well-developed radial wall jet region, but for conditions closer to the axis of symmetry errors of up to 18% were recorded as shown in Figure 5. The experiments show that $\delta_{1/2}$ varies linearly with r, while the calculations predict effectively the same trend as the experiments.

A detailed comparison of the radial velocity distributions at $r = 80$ and 120 mm for $H = 12D_n$ is shown in Figure 6 with suction velocities of $V_W = 0{\cdot}0$, 0·175 and 0·25 m s^{-1}. At these suction velocities the overall flow structure of the wall jet region is reasonably well predicted. It is obvious that the suction effect reduces the momentum boundary layer thickness and increases the velocity gradient near the surface. As might be expected, the agreement is much better towards the outer radii.

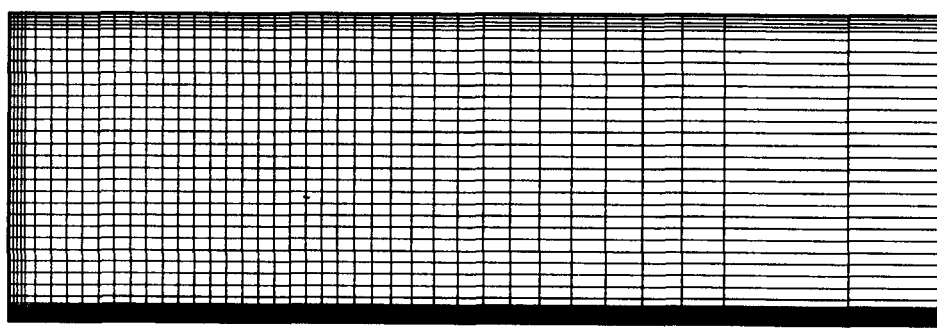

Figure 2

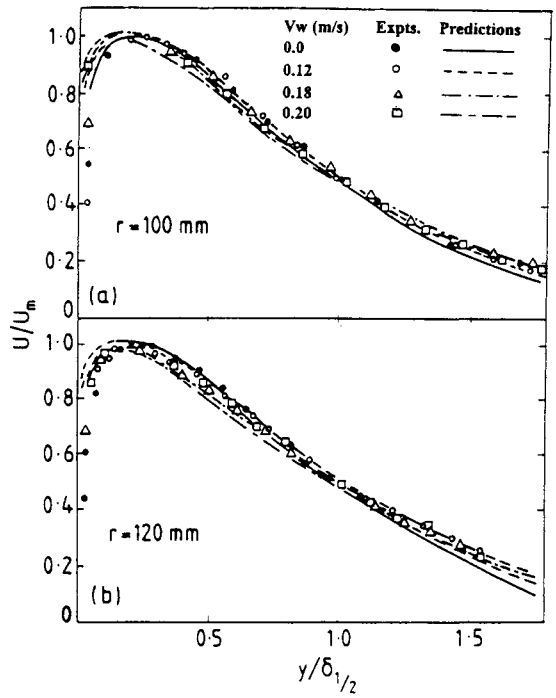

Figure 3

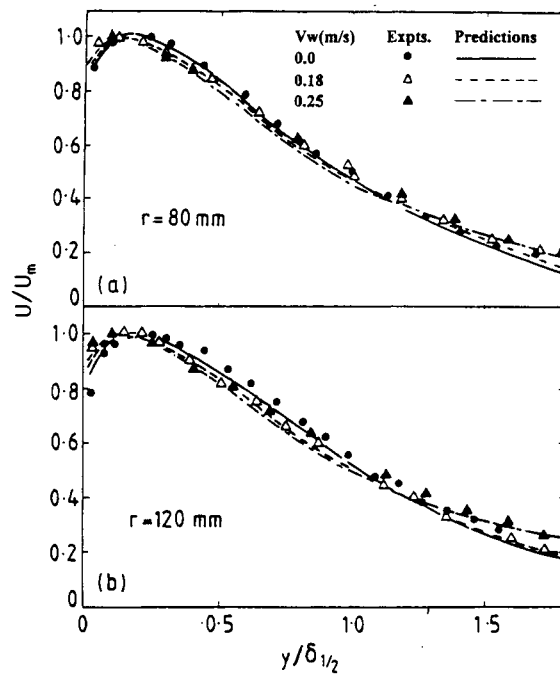

Figure 4

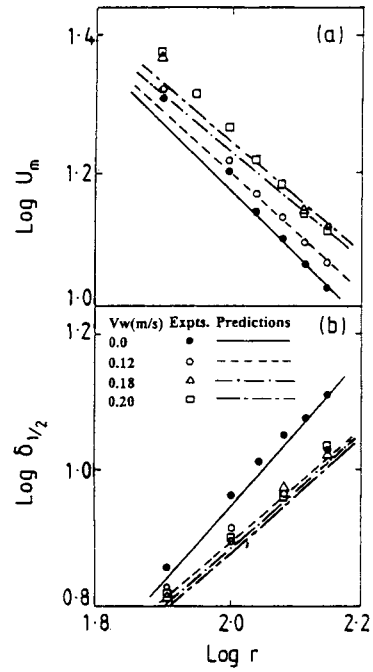

Figure 5

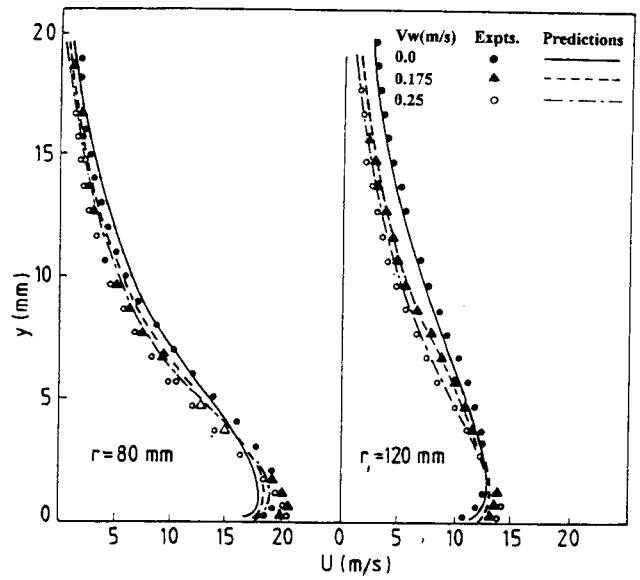

Figure 6

5. CONCLUSIONS

A computational procedure has been achieved by formulating the differential conservation equations governing the flow with the entrainment boundary. The method requires large amounts of computer time in order to predict the finer details of the flow with sufficient resolution. It is found that suction creates some volume of flow towards the impinging surface, reduces the momentum boundary layer thickness and correspondingly increases the velocity gradient near the surface. Certain discrepancies between the calculations and the available data may be caused by the isotropic assumption in the eddy viscosity/diffusivity model.

APPENDIX: NOMENCLATURE

C_μ, C_1, C_2	constants used in turbulence models
D_n	nozzle diameter
f	function defined by equation (2)
G	generation rate of turbulence kinetic energy
H	nozzle-to-wall distance
i	turbulence intensity
K	turbulence kinetic energy
P	pressure
r	co-ordinate in radial direction
r_n	nozzle radius
Re	nozzle Reynolds number
S_ϕ	source term of ϕ-equation
U	mean velocity component in x-direction
U_{cl}	velocity in direction of symmetry axis of flow
U_m	maximum radial velocity of wall region
U_n	nozzle exit velocity
U_τ	friction velocity
$V646$	mean velocity component in r-direction
V_W	suction velocity
x	co-ordinate in jet axial direction
y^+	distance from wall
$Y646$	radial width of mixing region

Greek letters

Γ_ϕ	diffusion coefficient of ϕ-equation
$\delta_{1/2}$	jet halfwidth for wall jet region
ε	turbulence energy dissipation rate
κ	Von Karman constant
λ	length scale constant
μ	dynamic viscosity
μ_{eff}	effective viscosity
μ_t	turbulent dynamic viscosity
ρ	density
σ_k	Prandtl number for turbulence kinetic energy
σ_ε	Prandtl number for energy dissipation rate
τ	total shear stress
τ_W	wall shear stress
ϕ	dependent variables (U, V, K and ϕ)

REFERENCES

1. M. B. Glauert, 'The wall jet', *J. Fluid Mech.*, **1**, 625–643 (1956).
2. M. Poreh, Y. G. Tsuei and J. E. Cermak, 'Investigation of turbulent radial wall jet', *J. Appl. Mech.*, **89**, 457–463 (1967).
3. S. C. Kacker and J. H. Whitelaw, 'The turbulence characteristics of two dimensional wall-jet and wall-wake flows', *J. Appl. Mech.*, **38**, 239 (1971).
4. K. H. Ng and D. B. Spalding, 'Turbulence model for boundary layers near walls', *Phys. Fluids*, **15**, (1972).
5. S. Beltaos and N. Rajaratnam, 'Plane turbulent impinging jet', *J. Hydraul. Res.*, **11**, (1973).
6. S. Beltaos and N. Rajaratnam, 'Impinging circular turbulent jets', *ASCE, J. Hydraul. Div.*, **100**, 1313–1328 (1974).
7. A. P. Govindan and R. K. Subba, 'Hydrodynamics of radial wall jets', *J. Appl. Mech.*, **41**, 518–519 (1974).
8. N. Rajaratum, *Turbulent Jets*, Elsevier, Amsterdam, 1976.
9. R. N. Sharma and S. V. Patankar, 'Numerical computations of wall jet flow', *Int. J. Heat Mass Transfer*, **25**, 1709–1718 (1982).
10. N. T. Obot, W. J. M. Douglas and A. S. Mujumdar, 'Influence of suction on the developing wall flow of an impinging jet', *AIAA J.*, **21**, 1774–1776 (1983).
11. B. E. Launder and D. B. Spalding, 'The numerical computation of turbulent flows', *Comput. Methods Appl. Mech. Eng.*, **3**, 269–289 (1974).
12. P. Bradshaw, *Turbulence*, 1976.
13. S. V. Patankar, *Numerical Heat Transfer and Fluid Flow*, McGraw-Hill, New York, 1980.